

A Study of the Numerical Stability of an ImEx Scheme with Application to the Poisson-Nernst-Planck Equations

M.C. Pugh*

*Department of Mathematics, University of Toronto,
40 St George St, Toronto, ON M5S 2E4, Canada*

David Yan

Department of Electrical and Computer Engineering, University of Toronto

F.P. Dawson

Department of Electrical and Computer Engineering, University of Toronto

Abstract

The Poisson-Nernst-Planck equations with generalized Frumkin-Butler-Volmer boundary conditions (PNP-FBV) describe ion transport with Faradaic reactions and have applications in a wide variety of fields. We solve the PNP-FBV equations using an adaptive time-stepper based on a second-order variable step-size, semi-implicit, backward differentiation formula (VSSBDF2). When the underlying dynamics are such that the solutions converge to a steady-state solution, we observe that the adaptive time-stepper produces solutions that “nearly” converge to the steady state and that, simultaneously, the time-step sizes stabilize to a limiting size dt_∞ . Linearizing the SBDF2 scheme about the steady state solution, we demonstrate that the linearized scheme is conditionally stable and that this is the cause of the adaptive time-stepper’s behaviour. Mesh-refinement, as well as a study of the eigenvectors corresponding to the critical eigenvalues, demonstrate that the conditional stability is not due to a time-step restriction caused by high-frequency contributions. We study the stability domain of the linearized scheme and find that its boundary can have corners as well as jump discontinuities. A jump discontinuity means there can be parameter values, ϵ_1 and ϵ_2 , that are very close to one another and a time-step size dt so that the computation of the ϵ_1 problem is stable and the computation of the ϵ_2 problem is unstable.

Keywords: Poisson-Nernst-Planck Equations; Semi-Implicit Methods; ImEx Methods; SBDF2; Adaptive time-stepping; Conditional Linear Stability

*Corresponding author

Email address: mpugh@math.utoronto.ca (M.C. Pugh)

1. Introduction

The Poisson-Nernst-Planck (PNP) equations are a parabolic-elliptic system that models the transport of charged species subject to diffusion and electromigration. The generalized Frumkin-Butler-Volmer (FBV) boundary conditions are nonlinear boundary conditions that model chemical reactions at the electrodes. The PNP equations model the behaviour in the bulk; the electrodes are located at the boundary of the “bulk” domain. There is a singular perturbation parameter ϵ ; small values of ϵ lead to thin boundary layers with sharp transitions to the behaviour in the bulk.

The PNP-FBV system is both nonlinear and diffusive. Hence a semi-implicit (also known as implicit-explicit) time-stepping scheme is a natural approach to take in hopes of avoiding stability restrictions on the time-step size while also avoiding the computational slowness caused by having to solve nonlinear equations. The linear diffusive term is handled implicitly and the nonlinear terms are handled explicitly. In this article, we study the stability properties of a second-order semi-implicit backwards differencing formula (SBDF2) as applied to the PNP-FBV system and find that the SBDF2 scheme becomes conditionally stable as the underlying solution of PNP-FBV system equilibrates.

The PNP-FBV system can be forced at one of the boundaries using either an imposed voltage or imposed current. Simulations considered a variety of imposed voltages and imposed currents; the adaptive time-stepper was vital in that it could refine, and subsequently coarsen, the time-steps in response to fast changes in the imposed forcing [1, 2]. The adaptive time-stepper presented in [1] is based on a second-order variable step-size, semi-implicit, backward differentiation formula (VSSBDF2 [3]). In the companion article [4], the adaptive VSSBDF2 time-stepper is presented in full and its speed and stability properties are compared to those of an adaptive time-stepper based on a second-order variable step-size, *fully-implicit*, backward differentiation formula (VSBDF2 [3]). It is demonstrated that for “large” values of the singular perturbation parameter ϵ , the (semi-implicit) VSSBDF2 adaptive time-stepper is faster and for “small” values of ϵ the (fully-implicit) VSBDF2 adaptive time-stepper is faster.

When the imposed forcing is held constant, and the underlying physical solution relaxes to a steady-state solution, the expected behaviour of an adaptive time-stepper is that the time-steps will grow until they reach the user-specified maximum time-step size, dt_{\max} , and the numerical solution will converge to the numerical steady state. This is precisely what is observed with the VSBDF2 adaptive time-stepper based on the fully-implicit BDF2 scheme [4]. However, we found that the VSSBDF2 adaptive time-stepper based on the semi-implicit SBDF2 scheme did not behave in the expected manner. Instead, as shown in Figure 1, we observe that the numerical solution gets close to, but fails to converge to, the numerical steady state and, simultaneously, the time-step sizes stabilize to a limiting step size dt_{∞} . (The figure only shows the behaviour up

to $t = 1.5$, however the observed behaviour continues past this time for as long as we chose to compute the solution.) Figure 1 is discussed fully in Section 4.

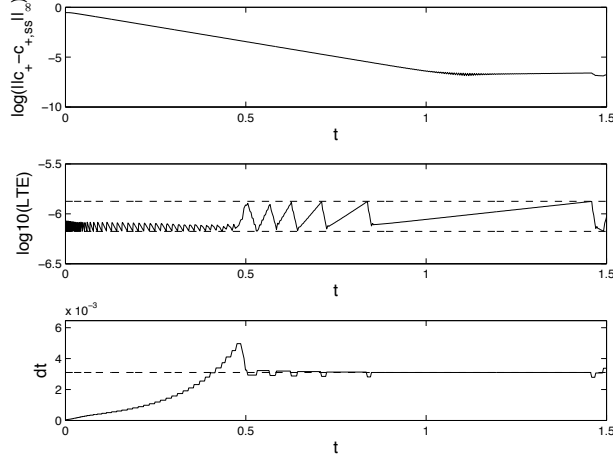


Figure 1: PNP-FBV system (1)–(8) with constant imposed voltage $v(t) = 2$, $\epsilon = .05$, and all other physical parameters set to 1. The spatial mesh is uniform, $dx = 1/90$. The initial data is $c_{\pm}(x, 0) = 1 + .1 \sin(2\pi x)$ and $\phi_x(1, 0) = 0$. The VSSBDF2 adaptive time-stepper is used. Top plot: Comparison of the solutions found by the VSSBDF2 adaptive time-stepper to the pre-computed numerical steady-state solution. Plot is $\log(\|c_+^n - c_{+,ss}\|_\infty)$ versus t_n . Deviations of c^n and ϕ^n from the corresponding steady state profiles behave similarly, as do their time derivatives as approximated using (10). Middle plot: The logarithm of the approximate local truncation error, (12), is plotted versus time. The dashed lines indicate the constraints set by the adaptive time-stepper: $\log(tol \pm range)$. See Appendix Appendix A. Bottom plot: Time-step size, dt , plotted versus time. The timestep sizes stabilize to a limiting value, denoted dt_∞ . The dashed line indicates the stability restriction $dt^* = 3.1000 \times 10^{-3}$ computed using the linear stability analysis presented in Section 5.

When the VSSBDF2 adaptive time-stepper is taking (essentially) constant time steps it is effectively an SBDF2 time-stepper with time-steps equal to dt_∞ . For for this reason, to try and understand the unexpected behaviour of the VSSBDF2 adaptive time-stepper, we perform a stability analysis of the SBDF2 scheme linearized about the steady-state solution. A significant challenge is that the linearized scheme cannot be reduced via diagonalization to a study of the scheme’s behaviour for a single linear ODE.

We demonstrate that the linearized scheme is conditionally stable with a stability restriction dt^* . Depending on the physical parameter values, when $dt = dt^*$, either there is one eigenvector with eigenvalue -1 or there is a pair of eigenvectors with complex eigenvalues of magnitude 1. The eigenvectors are not highly oscillatory and, when performing the stability analysis using different spatial discretizations, we find that the stability restriction, dt^* , does not change significantly. Specifically, dt^* does not go to zero as dx goes to zero; this shows that the conditional stability is not of “diffusive type” in which high frequencies

can grow exponentially in time if dt is too large.

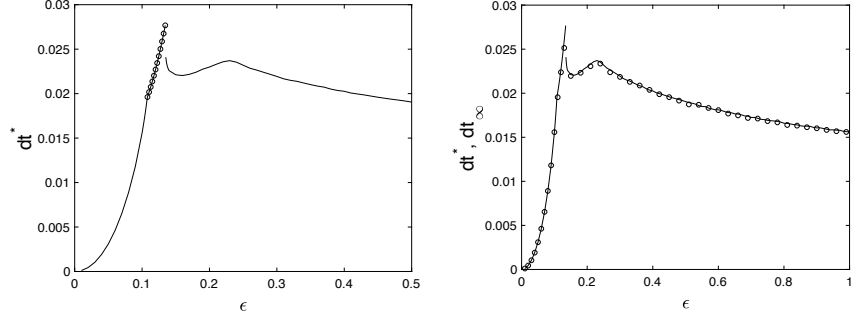


Figure 2: PNP-FBV system (1)–(8) with physical and numerical parameters identical to those used for Figure 1 except for ϵ , which varies. Left plot: Solid line: dt^* versus ϵ where dt^* is found from the linear stability analysis. Open circles denote ϵ values for which the time-step stability restriction arises from a pair of complex conjugate eigenvalues on the unit circle: $\epsilon \in (0.107764, 0.134504)$. Right plot: Solid line: dt^* versus ϵ where dt^* is found from the linear stability analysis. Open circles: dt_∞ as found by the time-step size stabilizing in the VSSBDF2 adaptive time-stepper.

The PNP-FBV system has a singular perturbation parameter ϵ . By varying ϵ , we are able to study how the stability restriction, dt^* , depends on ϵ . Figure 2 presents the graph of $(\epsilon, dt^*(\epsilon))$. We refer to the region below the graph as the “stability domain” of the SBDF2 scheme linearized about the state solution of the PNP-FBV system. We find that the stability domain is not smooth — there can be corners and jump discontinuities in the graph of dt^* ; see the left plot in Figure 2. Jump discontinuities are especially striking because they mean that the same value of dt could yield a stable SBDF2 computation for one value of ϵ but could result in a computation that blows up for another, close value of ϵ . We have not seen this type of phenomenon (non-smooth stability domains) reported in the literature. We find that for small values of ϵ the stability domain is not significantly influenced by the value of the (constant) imposed voltage or imposed current.

Our simulations suggest that $dt_\infty = dt^*$: the VSSBDF2 adaptive time-stepper is *finding* the stability restriction for the SBDF2 scheme. The right plot of Figure 2 presents the limiting time-step found by the adaptive time-stepper (dt_∞ , open circles) as well as the stability restriction (dt^* , solid line). The Figure is fully discussed in Section 5.

The VSSBDF2 adaptive time-stepper can be used with, or without, a Richardson extrapolation step (A.1). Richardson extrapolation is a common way to increase the accuracy of a scheme. In [5], we demonstrate that Richardson extrapolation can affect the linear stability of a scheme in various ways. There, we give an example of a PDE for which the SBDF2 scheme is unconditionally stable however, when used in combination with a Richardson extrapolation step, the time-stepping scheme is conditionally stable.

Time-step Stability Restrictions

Time-step stability restrictions can arise in a variety of ways. This article is not about stiffness in the sense of there being a restriction on the time-step size due to physical effects such as fast time scales. Rather, it is about a system in which the fast time scales that arise from discretizing the diffusion terms are well-handled by a commonly-used semi-implicit scheme. However, as the solution equilibrates, the scheme becomes conditionally stable, leading to a time-step restriction.

There have been many approaches to the challenge of “stiffness reduction” whether in semi-implicit linear multi-step methods [6, 7, 8, 9, 10, 11, 12, 13], Runge-Kutta methods [14, 15, 16], matrix exponential/integrating factor methods [17, 18, 19], and other approaches [20, 21, 22, 23]. These citations are provided as examples of the many seminal/well-written works in a large literature on the topic. It is likely that some of the methods proposed in the cited works could allow one to use knowledge of the structure of the linearized operator about the steady-state solution so as to modify the time-stepping scheme and remove the conditional stability.

Relevance of this work to other PDEs and other time-stepping schemes

In this article, we study the stability domain of the fixed-time-step SBDF2 scheme for the PNP-FBV system using a VSSBDF2 adaptive time-stepper. We then confirm, and better understand, the findings by studying a linearization of the SBDF2 scheme. This two-pronged approach of using both an adaptive time-stepper and a linearization study is not restricted to the PNP-FBV system or to the VSSBDF2, SBDF2 pairing.

We used the VSSBDF2 adaptive time-stepper on several dissipative systems that have non-constant, asymptotically stable steady states. For example, we found that a basic reaction diffusion equation, $u_t = u_{xx} \pm u^2$, did not yield a conditionally stable scheme when the SBDF2 scheme is linearized around the asymptotically stable steady state. However, we did find some simple models related to the PNP-BDF system with asymptotically stable steady states for which the SBDF2 scheme is conditionally stable when linearized about them [1]. The structure of the stability domain is also problem-specific. We considered some other dissipative systems and did not find stability domains with corners, cusps, or jumps (otherwise we would have presented results for a simpler system than the PNP-FBV system).

In terms of time-steppers, if one is using a linear multistep method (LMM) to study a physical system that has asymptotically stable steady states, our approach is relevant in the following ways.

- By using an adaptive time-stepper that is built upon the variable step-size version of the LMM, one is freed from needing to guess a “good” time-step size for a fixed-time-step scheme. Either the time-steps will get larger and larger as the solution converges to the steady state or they will stabilize to some limiting value dt_∞ . In the latter case, if one wishes to compute the numerical steady-state solution up to round-off error, one then can do this

with confidence by using the constant-time-step scheme with a time-step size chosen smaller than dt_∞ .

- We give a heuristic argument based on the local truncation error as to why, in general, an adaptive time-stepper would naturally find the stability restriction if the underlying constant-time-step scheme is conditionally stable when linearized about the steady state. As a result, if one builds an adaptive time-stepper based on a variable step-size version of the LMM being used, one can use the adaptive time-stepper to explore the stability domain of the constant-step-size LMM. If, when computing an initial value problem, the time-step size stabilizes to a value dt_∞ , this suggests that the underlying constant-time-step scheme is conditionally stable when linearized about the steady state, with stability restriction dt^* and $dt_\infty = dt^*$.
- If the constant-step-size LMM is conditionally stable when linearized about the steady state, one needs to study the eigenvalues of the linearized problem in order to understand stability domain features such as corners, jumps, and whether or not it is a single real-valued eigenvalue that goes unstable as dt exceeds dt^* . The procedure we use to linearize about the steady state and find the eigenvalues and eigenvectors of the linearized system could be used for any LMM.

1.1. Structure of the article

This article is structured as follows. Section 2 presents the PNP-FBV system. Section 3 presents an overview of the adaptive time-stepper. Section 4 presents the numerical simulations of the an initial value problem. In Section 5, the linearization about the steady-state solution is presented. In Subsection 5.1, the process for finding the stability restriction dt^* is discussed. The dependence of the stability restriction dt^* on physical quantities such as the singular perturbation parameter ϵ and the imposed voltage are discussed in Subsections 5.2 and 5.3 respectively. The dependence of the stability restriction dt^* on numerical aspects such as the mesh and whether or not Richardson extrapolation is used are discussed in Subsections 5.4 and 5.5 respectively.

2. The PNP-FBV system

The Poisson-Nernst-Planck (PNP) equations describe the transport of charged species subject to diffusion and electromigration. They have wide applicability in electrochemistry, and have been used to model a number of different systems, including porous media [24, 25, 26, 27], microelectrodes [28, 29], ion-exchange membranes [30, 31], electrokinetic phenomena [32, 33, 34], ionic liquids [35, 36], electrochemical thin films [37, 38, 39], fuel cells [40], supercapacitors [41], and many more. The Frumkin-Butler-Volmer boundary conditions describe charge transfer reactions at electrodes.

The one-dimensional, nondimensionalized PNP equations for a medium with 2 mobile species is

$$\frac{\partial c_{\pm}}{\partial t} = -\frac{\partial}{\partial x} \left[-\frac{\partial c_{\pm}}{\partial x} - z_{\pm} c_{\pm} \frac{\partial \phi}{\partial x} \right], \quad t > 0, x \in (0, 1), \quad (1)$$

$$-\epsilon^2 \frac{\partial^2 \phi}{\partial x^2} = \frac{1}{2} (z_+ c_+ + z_- c_-), \quad x \in (0, 1), \quad (2)$$

where c_{\pm} and z_{\pm} are the concentration and charge number of the positive/negative ion, ϕ is the potential and ϵ is the ratio of the Debye screening length to the inter-electrode width L . This width is used in the nondimensionalization of the original modelling equations [2]; the domain $(0, L)$ is rescaled to $(0, 1)$. We consider a model in which the anion and cation have a single charge ($z_{\pm} = \pm 1$) and the anion has no charge-transfer reactions at the electrode: c_- has no-flux boundary conditions:

$$-\left(-\frac{\partial c_-}{\partial x} + c_- \frac{\partial \phi}{\partial x} \right) \Big|_{x=0} = \left(-\frac{\partial c_-}{\partial x} + c_- \frac{\partial \phi}{\partial x} \right) \Big|_{x=1} = 0. \quad (3)$$

The cation is assumed to have a reaction at the electrodes involving the transfer of one electron; this is modelled using generalized Frumkin-Butler-Volmer (FBV) boundary conditions:

$$-\left(-\frac{\partial c_+}{\partial x} - c_+ \frac{\partial \phi}{\partial x} \right) \Big|_{x=0} = F(t) := 4k_{c,a} c_+(0, t) e^{-0.5 \Delta \phi_{\text{left}}} - 4j_{r,a} e^{0.5 \Delta \phi_{\text{left}}}, \quad (4)$$

$$\left(-\frac{\partial c_+}{\partial x} - c_+ \frac{\partial \phi}{\partial x} \right) \Big|_{x=1} = G(t) := 4k_{c,c} c_+(1, t) e^{-0.5 \Delta \phi_{\text{right}}} - 4j_{r,c} e^{0.5 \Delta \phi_{\text{right}}}, \quad (5)$$

where $k_{c,a}$, $k_{c,c}$, $j_{r,a}$, and $j_{r,c}$ are reaction rate parameters; the second part of the subscripts a and c refer to the anode and cathode, respectively. Equations (4)–(5) model the electrodeposition reaction $C^+ + e^- \rightleftharpoons M$ where M represents the electrode material. The Stern layer is a compact layer of charge that occurs in the electrolyte next to an electrode surface [42, 43]; λ_S denotes the effective width of this layer. In equations (4)–(5), $\Delta \phi_{\text{left}}$ and $\Delta \phi_{\text{right}}$ refer to the potential differences across the Stern layers that occur at the anode and cathode respectively. Specifically,

$$\Delta \phi_{\text{left}} = \phi_{\text{anode}} - \phi(0, t) = -\phi(0, t), \quad \Delta \phi_{\text{right}} = \phi_{\text{cathode}} - \phi(1, t) = v(t) - \phi(1, t) \quad (6)$$

where the potential at the anode has been set to zero and $v(t)$ denotes the potential at the cathode. In addition, the Poisson equation (2) uses a mixed (or Robin) boundary condition [37, 38, 39],

$$-\epsilon \delta \frac{\partial \phi}{\partial x} \Big|_{x=0} = \Delta \phi_{\text{left}} := -\phi(0, t), \quad (7)$$

$$+\epsilon \delta \frac{\partial \phi}{\partial x} \Big|_{x=1} = \Delta \phi_{\text{right}} := v(t) - \phi(1, t), \quad (8)$$

where $\delta = \lambda_S/L$. Finally, there is an ODE which ensures conservation of electrical current at the electrode [44, 45],

$$-\frac{\epsilon^2}{2} \frac{d}{dt} \phi_x(1, t) = j_{\text{ext}}(t) - [k_{c,c} c_+(1, t) e^{-0.5 \Delta \phi_{\text{right}}} - j_{r,c} e^{0.5 \Delta \phi_{\text{right}}}], \quad (9)$$

where $j_{\text{ext}}(t)$ is the external current. We refer to the PNP equations with the generalized Frumkin-Butler-Volmer boundary conditions as the PNP-FBV system.

The device is operated in two regimes — either the current or the voltage at the cathode is externally controlled¹. If the voltage at the cathode, $v(t)$, is imposed then the the PNP-FBV system (1)–(2) with boundary conditions (3)–(5) and (6)–(8) are numerically solved, determining c_{\pm} and ϕ . The current is found a posteriori using equation (9). If the current, $j_{\text{ext}}(t)$, is imposed then the ODE (9) is part of the PNP-FBV system and is numerically solved along with the PDEs, determining c_{\pm} , ϕ , and $\phi_x(1, t)$ simultaneously. The voltage $v(t)$ is then found a posteriori.

3. The adaptive time-stepper

The companion article [4] and [1] present the numerical scheme in full: spatial discretization, boundary conditions, splitting scheme, and error control.

The method of lines is used to discretize the parabolic PDEs (1). The spatial discretization reduces the parabolic-elliptic system of PDEs to a differential-algebraic system of equations. The system is handled using a splitting method: the ODEs are time-stepped, the system of algebraic equations is solved, the ODEs are time-stepped again, and so forth.

The linear diffusion terms in the parabolic PDEs (1) yield stiff linear terms in the ODEs. The terms in (1) that model electromigration are nonlinear, yielding nonlinear terms in the ODEs. The nonlinear terms make using implicit time-stepping methods unappealing. Semi-implicit, or implicit-explicit schemes, are often used for stiff problems as a way to avoid a fully-implicit treatment.

Consider the ODE $u' = g(u) + f(u)$ where $g(u)$ is a stiff linear term and $f(u)$ is a nonlinear term. Given u^{n-1} at time $t^{n-1} = t^n - dt$ and u^n at time t^n , the SBDF2 scheme determines u^{n+1} at time $t^{n+1} = t^n + dt$ via

$$\text{SBDF2: } \frac{1}{dt} \left(\frac{3}{2} u^{n+1} - 2 u^n + \frac{1}{2} u^{n-1} \right) = g(u^{n+1}) + 2 f(u^n) - f(u^{n-1}), \quad (10)$$

where u^n approximates $u(t^n)$ (see, for example, [46]). Our VSSBDF2 adaptive time-stepper is based on a second-order variable step-size semi-implicit backwards differencing formula, introduced by Wang and Ruuth [3], as a generaliza-

¹We use “imposed” as short-hand for externally controlled.

tion of the SBDF2 scheme:

$$\begin{aligned} \text{VSSBDF2: } \quad \frac{1}{dt_{\text{now}}} \left(\frac{1+2\omega}{1+\omega} u^{n+1} - (1+\omega)u^n + \frac{\omega^2}{1+\omega} u^{n-1} \right) \\ = g(u^{n+1}) + (1+\omega)f(u^n) - \omega f(u^{n-1}), \end{aligned} \quad (11)$$

where $\omega = dt_{\text{now}}/dt_{\text{old}}$, u^{n-1} is at time $t^{n-1} = t^n - dt_{\text{old}}$, and u^{n+1} is at time $t^{n+1} = t^n + dt_{\text{now}}$. Note that if $dt_{\text{now}} = dt_{\text{old}}$, VSSBDF2 reduces to SBDF2.

The VSSBDF2 adaptive time-stepper is described in detail in the companion article [4]; see also [1]. The key idea is: if one has computed the (approximate) solution up to the current time, (u^l, t^l) for $l = 0, \dots, n$, one can use these solutions and the time-stepper to choose a new time t^{n+1} so that the local truncation error $|u^{n+1} - u(t^{n+1})|$ is “small but not too small”.

One cannot know the local truncation error if one does not know the (exact) solution $u(t^{n+1})$; in practice one needs an approximation of the local truncation error. We do this by performing a “coarse” time step and a “fine” time step to compute u_c^{n+1} and u_f^{n+1} , respectively, and then using equation (12) to approximate the truncation error ϵ_c^{n+1} .

$$\epsilon_c^{n+1} = \frac{8(dt_{\text{old}} + dt_{\text{now}})}{7dt_{\text{old}} + 5dt_{\text{now}}} \left(u_c^{n+1} - u_f^{n+1} \right) \approx u_c^{n+1} - u(t^{n+1}). \quad (12)$$

If the error is acceptable, we advance in time. If the error is unacceptable, we choose a new dt_{now} and try again. If dt_{now} has been accepted, we take $u^{n+1} = u_c^{n+1}$. An algorithmic overview is given in Appendix A. A detailed discussion of the adaptive time stepping and error control schemes can be found in [1, 4].

This section describes the approach for an ODE; $u^n \in \mathbb{R}$. It generalizes immediately to a system of ODEs with $\mathbf{u}^n \in \mathbb{R}^N$.

4. Simulations of the PNP-FBV system

Figure 1 presents a simulation of an initial value problem for the PNP-FBV system (1)–(8) with constant imposed voltage. The initial data is fixed, as are all the other physical parameters. Solutions are computed using the VSSBDF2 adaptive time-stepper.

The top plot in the figure demonstrates that, after a short transient, the solution initially decays exponentially quickly to a numerical steady state. However, once the solution is within (approximately) 10^{-7} of the steady-state solution, this convergence ends and the computed solution stays about 10^{-7} away from the steady state. The middle plot in the figure demonstrates that the VSSBDF2 adaptive time-stepper is keeping the (approximate) local truncation error (12) within the user-specified interval. The bottom plot in the figure demonstrates that the time-step size initially increases exponentially fast and after a while it decreases and stabilizes to dt_{∞} . The dashed line in the bottom figure is the

stability restriction found by the linear stability analysis discussed in Section 5: dt^* . This simulation demonstrates that the VSSBDF2 adaptive time-stepper appears to eventually stabilize at a time-step size that is precisely the stability restriction.

The top plot presents the logarithm of the norm of the deviation of \mathbf{c}_+ from the numerical steady state $\mathbf{c}_{+,ss}$; that is $\log(\|\mathbf{c}_+^n - \mathbf{c}_{+,ss}\|)$. The deviations of \mathbf{c}_-^n and ϕ^n from the respective numerical steady states behave similarly. The numerical steady state, $\mathbf{c}_{\pm,ss}$ and ϕ_{ss} , satisfies the discretized version of the steady-state equations $0 = c_{\pm,xx} + z_{\pm}(c_{\pm}\phi_x)$ and (2). To find them, a simulation using the VSSBDF2 adaptive time-stepper is stopped once the time steps have stabilized. The SBDF2 time-stepper is then used to continue the simulation with a (fixed) time-step dt chosen to be smaller than dt_{∞} . The local truncation error tends to zero exponentially fast and the simulation is stopped once the computed solution satisfies the discretized steady-state equations (up to round-off). This late-time solution is taken as the numerical steady-state solution.

If, rather than studying the deviations, one approximates the time derivative, $\mathbf{c}_{+,t}$, using (11), then the plot of $\log(\|\mathbf{c}_{+,t}\|)$ versus t will show that $\|\mathbf{c}_{+,t}\|$ decreases and then stabilizes at a *nonzero* value.

Two of the user-specified parameters of an adaptive time-stepper are dt_{\min} and dt_{\max} . The time-stepper is not allowed to take dt smaller than dt_{\min} or larger than dt_{\max} . The above-described behaviour is what is observed if $dt_{\infty} < dt_{\max}$. If, by chance, it happens that dt_{\max} is smaller than dt_{∞} then as the solution equilibrates the time steps increase to dt_{\max} and are then held at that value. The solution subsequently converges to the steady-state solution.

Rosam, Jimack and Mullis [47] used an adaptive SBDF2 algorithm to study a problem in binary alloy solidification. In their Figure 4, they appear to show time-steps stabilizing to a constant value, but the reason is not given: they report that it is related to the tolerance set in the adaptive time-stepper. We did not observe such a phenomenon when we varied tol ; we found the same limiting time-step size dt_{∞} . Also, we find that decreasing tol leads to the deviations becoming smaller before levelling out (see top plot of Figure 1).

5. Numerical Linear Stability

If the imposed voltage or imposed current is constant for a period of time and if dt_{\max} is large, then the solution attempts to equilibrate and the VSSBDF2 adaptive time-stepper stabilizes to take (nearly) constant time steps dt_{∞} . The VSSBDF2 scheme with constant time steps is the SBDF2 scheme; for this reason we study the SBDF2 time-stepper to try and understand this stabilization of the VSSBDF2 adaptive time-stepper.

Consider the SBDF2 scheme (10) applied to the N ODEs $\mathbf{u}_t = \mathbf{f}(\mathbf{u}) + \mathbf{g}(\mathbf{u})$ that arise from spatially discretizing the PDE $u_t = f(u, u_x, u_{xx}, \dots) +$

$g(u, u_x, u_{xx}, \dots)$:

$$\frac{1}{dt} \left(\frac{3}{2} \mathbf{u}^{n+1} - 2\mathbf{u}^n + \frac{1}{2} \mathbf{u}^{n-1} \right) = \mathbf{g}(\mathbf{u}^{n+1}) + 2\mathbf{f}(\mathbf{u}^n) - \mathbf{f}(\mathbf{u}^{n-1}). \quad (13)$$

The bold-faced quantities are vectors in \mathbb{R}^N . A steady state satisfies $0 = \mathbf{g}(\mathbf{u}_{ss}) + \mathbf{f}(\mathbf{u}_{ss})$. Linearizing about \mathbf{u}_{ss} yields

$$\frac{1}{dt} \left(\frac{3}{2} \mathbf{d}^{n+1} - 2\mathbf{d}^n + \frac{1}{2} \mathbf{d}^{n-1} \right) = \mathbf{J}_{\mathbf{g}}(\mathbf{u}_{ss}) \mathbf{d}^{n+1} + 2\mathbf{J}_{\mathbf{f}}(\mathbf{u}_{ss}) \mathbf{d}^n - \mathbf{J}_{\mathbf{f}}(\mathbf{u}_{ss}) \mathbf{d}^{n-1}. \quad (14)$$

where $\mathbf{d}^m = \mathbf{u}^m - \mathbf{u}_{ss}$ is the deviation from the steady state and $\mathbf{J}_{\mathbf{f}}(\mathbf{u}_{ss})$ and $\mathbf{J}_{\mathbf{g}}(\mathbf{u}_{ss})$ are the Jacobian matrices evaluated at \mathbf{u}_{ss} ; e.g. $(\mathbf{J}_{\mathbf{f}}(\mathbf{u}_{ss}))_{ij} = \frac{\partial f_i}{\partial u_j}(\mathbf{u}_{ss})$. For simple problems, $\mathbf{J}_{\mathbf{f}}$ and $\mathbf{J}_{\mathbf{g}}$ can be determined analytically and evaluated at \mathbf{u}_{ss} . Otherwise, one can numerically approximate $\mathbf{J}_{\mathbf{f}}(\mathbf{u}_{ss})$ and $\mathbf{J}_{\mathbf{g}}(\mathbf{u}_{ss})$ in a variety of ways. We used a simple centre-difference scheme.

If the Jacobian matrices, $\mathbf{J}_{\mathbf{f}}(\mathbf{u}_{ss})$ and $\mathbf{J}_{\mathbf{g}}(\mathbf{u}_{ss})$, can be simultaneously diagonalized, then the system (14) reduces to a decoupled system of second-order difference equations. In this case, the stability analysis is straight-forward: one computes the roots of the now-decoupled difference equations and analytically studies how they depend on dt and the eigenvalues of $\mathbf{J}_{\mathbf{f}}(\mathbf{u}_{ss})$ and $\mathbf{J}_{\mathbf{g}}(\mathbf{u}_{ss})$. Indeed, in Appendix A of [5], we present the linear stability analysis of (13) for a single linear ODE. We use it to study the logistic equation, demonstrating that the dt_{∞} found by the VSSBDF2 adaptive time-stepper is in sharp agreement with the analytically-determined stability restriction dt^* .

For the PNP-FBV system (1)–(8), the Jacobians *cannot* be simultaneously diagonalized. For this reason, we proceed with a numerical computation of the eigenvalues and eigenvectors of the linearized scheme (14) rewritten as

$$\mathbf{d}^{n+1} = M_{\text{new}} M_{\text{now}} \mathbf{d}^n + M_{\text{new}} M_{\text{old}} \mathbf{d}^{n-1}, \quad (15)$$

where

$$M_{\text{new}} = \left(\frac{3}{2} I - dt \mathbf{J}_{\mathbf{g}}(\mathbf{u}_{ss}) \right)^{-1}, M_{\text{now}} = 2I + 2dt \mathbf{J}_{\mathbf{f}}(\mathbf{u}_{ss}), M_{\text{old}} = -\frac{1}{2} I - dt \mathbf{J}_{\mathbf{f}}(\mathbf{u}_{ss}).$$

Equation (15) is a system of N second-order linear difference equations. Solving it requires the initial deviation, \mathbf{d}^0 , as well as the deviation after one time-step, \mathbf{d}^1 . The system is rewritten [48, §D.2.1] as $2N$ first-order linear difference equations in the standard manner: $\mathbf{D}^n := [\mathbf{d}^{n-1}; \mathbf{d}^n] \in \mathbb{R}^{2N}$ and A is the companion matrix for the difference equation:

$$\mathbf{D}^{n+1} = A \mathbf{D}^n = \begin{pmatrix} 0 & I \\ M_{\text{new}} M_{\text{old}} & M_{\text{new}} M_{\text{now}} \end{pmatrix} \mathbf{D}^n. \quad (16)$$

If $(\lambda_j, \mathbf{v}_j)$ is an eigenvalue-eigenvector pair of A then the structure of A implies that $\mathbf{v}_j = [\mathbf{d}_j; \lambda_j \mathbf{d}_j]$ for some $\mathbf{d}_j \in \mathbb{R}^N$. If A has $2N$ linearly independent

eigenvectors, it follows that the general solution of the linearized problem (14) is

$$\mathbf{d}^n = \sum_{j=1}^{2N} c_j \lambda_j^n \mathbf{d}_j \quad (17)$$

where the $2N$ coefficients, c_j , are determined using $\mathbf{d}^0, \mathbf{d}^1 \in \mathbb{R}^N$.

The connection between the linearized scheme (14) and the nonlinear scheme (13) is via the stability theory of fixed points for discrete dynamical systems. If $\mathbf{J}_{\mathbf{f}}$ and $\mathbf{J}_{\mathbf{g}}$ are continuous in a neighbourhood of \mathbf{u}_{ss} and if dt is such that $(\frac{3}{2}I - dt \mathbf{J}_{\mathbf{g}}(\mathbf{u}_{ss}))$ is invertible then the discrete dynamical system

$$\mathbf{U}^{n+1} = \mathbf{F}(\mathbf{U}^n) := \begin{pmatrix} \mathbf{U}_2^n \\ (\frac{3}{2}I - dt \mathbf{g})^{-1} (2\mathbf{U}_2^n + 2 dt \mathbf{f}(\mathbf{U}_2^n) - \frac{1}{2}\mathbf{U}_1^n - dt \mathbf{f}(\mathbf{U}_1^n)) \end{pmatrix} \quad (18)$$

is defined in a neighbourhood of the fixed point $[\mathbf{u}_{ss}; \mathbf{u}_{ss}]$. Defining $\mathbf{U}^{n+1} = [\mathbf{u}^n; \mathbf{u}^{n+1}]$, this discrete dynamical system (18) is equivalent to the SBDF2 time-stepping scheme (13). The companion matrix A is the linearization of (18) at the fixed point $[\mathbf{u}_{ss}; \mathbf{u}_{ss}]$. Therefore, if all eigenvalues of A have magnitude less than 1, then $[\mathbf{u}_{ss}; \mathbf{u}_{ss}]$ is an asymptotically stable fixed point of (18) and \mathbf{u}_{ss} is an asymptotically stable fixed point of the SBDF2 scheme (13).

5.1. Finding the stability restriction dt^* (if there is one)

Given a particular PDE (or set of PDEs) and boundary conditions, we compute the Jacobians (using the time-step dt that was used in the SBDF2 time-stepper to find u_{ss}) about the steady state and construct the matrix A in (16). The eigenvalues of A will have magnitude less than one — otherwise the time-stepper would not have found the steady-state solution. To determine if there is a linear stability restriction, one increases the time-step size, recomputes A and its eigenvalues, and then determines if any eigenvalues have magnitude greater than one for this new value of dt . Proceeding in this way, one seeks a time-step size at which an eigenvalue(s) crosses from magnitude less than one to magnitude greater than one. We use an iterative bisection method to approximate this critical time-step size, dt^* . The scheme is conditionally stable in that \mathbf{u}_{ss} is an asymptotically stable steady-state solution of the SBDF2 time-stepper if $dt < dt^*$ and is an unstable steady state if $dt > dt^*$.

Whether or not there is such a stability restriction on dt is a problem-specific question. And, of course, not finding dt^* could either indicate unconditional stability or it could indicate that one has not tried large enough values of dt .

The above process depends on first finding a value of dt such that u_{ss} is asymptotically stable under the dynamics (13). In practice, dt^* is not a priori known, and so the region $0 < dt < dt^*$ is unknown. For this reason, we first use the VSSBDF2 adaptive time-stepper. If it yields a solution that appears to be “trying to but failing to converge”² to a steady-state solution, we take

²That is, the local truncation error stays in the user-specified interval, the approximation

this as evidence of the SBDF2 scheme's being conditionally stable when linearized about the steady state. We then choose some $dt < dt_\infty$ and repeat the simulation using the (constant time-step) SBDF2 scheme to find a steady-state solution, as described in Section 4.

Turning to the PNP-FBV system (1)–(8), for a fixed constant imposed voltage and ϵ , we use the (constant time-step) SBDF2 time-stepper to find the discrete steady-state solution $\mathbf{c}_{+,ss}$, $\mathbf{c}_{-,ss}$, and ϕ_{ss} . The steady-state concentrations are concatenated into one vector $\mathbf{u}_{ss} := [\mathbf{c}_{+,ss}; \mathbf{c}_{-,ss}]$. The right-hand sides of the discretized evolution equations (1) are similarly concatenated: \mathbf{f} is the spatial discretization of $[(c_+ \phi_x)_x; (c_- \phi_x)_x]$ and \mathbf{g} is the discretization of $[c_{+,xx}; c_{-,xx}]$. We then approximate the Jacobians $\mathbf{J}_f(\mathbf{u}_{ss})$ and $\mathbf{J}_g(\mathbf{u}_{ss})$. If there are N mesh points then $\mathbf{u}_{ss} \in \mathbb{R}^{2N}$ and the Jacobians are $2N \times 2N$ matrices. A value of dt is chosen and the $4N \times 4N$ companion matrix A in (16) is constructed and its eigenvalues and eigenvectors are computed. The value of dt is then increased and the process is repeated.

Figure 3 presents results for $\epsilon = .05$ with constant imposed voltage. In the left figure, the magnitudes of all eigenvalues are plotted — we see that for small values of dt , all eigenvalues have magnitude less than one and that, as dt is increased, one branch goes unstable. We follow this branch to find the time-step size at which the magnitude equals 1; this is the stability restriction dt^* . We find that one eigenvalue crosses the unit circle, crossing at value -1 . In the top plot in the right figure, we plot the steady states $\mathbf{c}_{\pm,ss}$. In the bottom plot in the right figure, we plot the eigenvectors at the stability restriction dt^* . We refer to the eigenvector-eigenvalue pair as “barely stable”.

To demonstrate that the “barely stable” eigenvalue-eigenvector pair is the cause of the failure to converge to the steady state shown in the top plot of Figure 1, we took \mathbf{c}_+ and \mathbf{c}_- at a late time ($t = 100$) and computed the corresponding deviations from the steady state \mathbf{d}_+ and \mathbf{d}_- . In the bottom-right plot of Figure 3, the normalized deviations are plotted with open circles — note that they closely fit the “barely stable” eigenfunctions.

To see why it is unsurprising that the VSSBDF2 adaptive time-stepper would adjust its timesteps until they stabilize at the stability restriction of the underlying SBDF2 scheme, we consider the local truncation error for the SBDF2 scheme, applied to the ODE $u_t = f(u) + g(u)$, close to a steady state u_{ss} :

$$\begin{aligned} LTE &= u^{n+1} - u(t_{n+1}) = d^{n+1} - d(t_{n+1}) \\ &= \left(\frac{2}{3} d'''(t_n) - g''(u(t_n)) d'(t_n)^2 - g'(u(t_n)) d''(t_n) \right) dt^3 + O(dt^4). \end{aligned}$$

Here $u(t_n) = u^n$, $d(t_{n+1}) = u(t_{n+1}) - u_{ss}$, and $d^{n+1} = u^{n+1} - u_{ss}$. Assume the dynamics of the underlying system of ODES is that of solutions converging to an

of u_t decays exponentially and then stabilizes, and the time-step sizes are stabilizing at some value $dt_\infty < dt_{\max}$

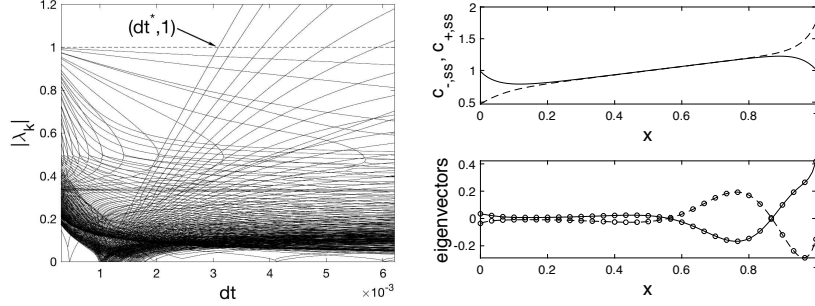


Figure 3: PNP-FBV system (1)–(8) with physical and numerical parameters identical to those used for Figure 1. Left plot: The magnitudes of the 364 eigenvalues are plotted versus dt . The largest magnitude branch crosses at $dt^* = .003094$. Right plot, top: The steady-state profiles — the solid line is $\mathbf{c}_{+,ss}$ and the dashed line is $\mathbf{c}_{-,ss}$. Right plot, bottom: At $dt = dt^*$, one real-valued eigenvalue is “barely stable”: $\lambda = -1$. The corresponding “barely stable” eigenvectors are plotted — the solid line is the eigenvector for \mathbf{c}_+ and the dashed line is the eigenvector for \mathbf{c}_- . Both eigenvectors have been chosen to have l^2 norm 1. The open circles denote late-time deviations from the steady states, as computed using the VSSBDF2 adaptive time-stepper. The deviations have been normalized to have l^2 norm 1; only a third of the $N = 91$ data points are plotted for tidiness.

asymptotically stable steady state. Now assume that the numerical approximations are also converging to the asymptotically stable steady state. In this situation, the deviation is decaying exponentially in time: $d(t) \cong C \exp(-\lambda t)$ and the local truncation error can be bounded

$$|C| \alpha e^{-\lambda t_n} dt^3 \leq |LTE| \leq |C| \beta e^{-\lambda t_n} dt^3 \quad (19)$$

where α and β are determined by λ and uniform bounds on g' and g'' near u_{ss} . The upper bound in (19) implies that if dt is held fixed, the LTE will decay to zero as $t_n \rightarrow \infty$. The lower bound in (19) implies that if the LTE is required to satisfy a constraint such as $LTE \geq tol - range > 0$, then dt must grow exponentially as $t_n \rightarrow \infty$.

Whether or not the numerical approximations are converging to the asymptotically stable steady state is determined by the spectral radius of the scheme linearized about the steady state. For a system of N ODEs, the spectral radius of the linearized scheme is

$$|\lambda(dt)|_{\max} = \max_{1 \leq i \leq N} \{|\lambda_i(dt)|\}.$$

If dt is such that $|\lambda(dt)|_{\max} < 1$, then the LTE for the SBDF2 scheme will go to zero exponentially fast as the number of time steps goes to infinity: the numerical approximations are converging to the asymptotically stable steady state. Similarly, if $|\lambda(dt)|_{\max} > 1$, then the LTE will grow exponentially until nonlinear effects become relevant. When our simulations with the VSSBDF2 adaptive time-stepper stabilize to dt_∞ , they are taking essentially-constant time-steps. At the same time, the LTE is constrained to stay in an interval $[tol -$

$range, tol+range]$ where $tol-range > 0$. This can only happen if $|\lambda(dt_\infty)|_{\max} = 1$; i.e., $dt_\infty = dt^*$.

There is nothing specific to the SBDF2 scheme and its variable step-size generalization VSSBDF2 in this argument. Any adaptive time-stepper that is built on a variable step-size generalization of a constant-step-size scheme could be used to explore the stability properties of the constant-step-size scheme.

5.2. Dependence of the stability domain on the singular perturbation parameter ϵ

We now consider the stability properties of the PNP-FBV system (1)–(8) for a range of values of ϵ , holding the imposed voltage and all other parameters fixed.. We find that for $\epsilon \in (0.107764, 0.134504)$ the instability takes the form of a pair of complex eigenvalue crossing the unit circle; for all other values we considered it was a single eigenvalue crossing at -1 . Figure 4 is the analogue of Figure 3 but for a value of ϵ that results in two complex eigenvalues crossing the unit circle.

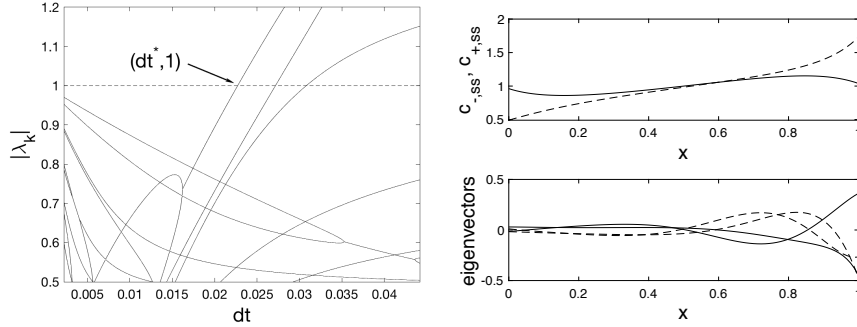


Figure 4: PNP-FBV system (1)–(8) with physical and numerical parameters identical to those used for Figure 1 except for $\epsilon = .12$. Left plot: The magnitudes of the 364 eigenvalues are plotted versus dt ; the vertical range has been truncated for a tidier plot. The largest magnitude branch crosses at $dt^* = .02271$. Right plot, top: The steady-state profiles — solid line is $c_{+,ss}$ and dashed line is $c_{-,ss}$. Right plot, bottom: A pair of complex-valued eigenvalues, $-0.9797 \pm 0.2008i$, go unstable. The corresponding eigenvectors are plotted — the solid lines are the unstable eigenvectors for c_+ and the dashed line are the unstable eigenvectors for c_- .

For each ϵ , we find the stability restriction dt^* . The left plot of Figure 2 presents dt^* as a function of ϵ . The open circles indicate the interval of ϵ values for which a pair of complex conjugate eigenvalues cross the unit circle. The stability restriction dt^* is a continuous function of ϵ except for a jump at $\epsilon \approx 0.134504$. Also, dt^* appears to be a smooth function of ϵ except at $\epsilon \approx 0.134504$ (where there is a jump in dt^*) and at $\epsilon \approx 0.107764$ (where there is a corner).

The jump in dt^* is striking — if one were using an SBDF2 time-stepper with $dt = .025$ then this would yield a stable simulation for ϵ which is close

to, but slightly smaller than, the critical value of $\epsilon \approx 0.134504$. The simulation would be unstable simulation for ϵ which is close to, but slightly larger than, this critical value. The stability of the SBDF2 simulation is not a continuous function of the parameter ϵ .

The right plot of Figure 2 compares dt_∞ as found from the VSSBDF2 adaptive time-stepper to dt^* as found from the linear stability study of the steady state. The solid line plots dt^* versus ϵ ; the circles plot dt_∞ . The circles align closely with the solid lines, providing compelling evidence that it is the numerical instability of the scheme near the steady state which is causing the VSSBDF2 adaptive time-stepper to stabilize its time-steps.

Figure 5 addresses the cause of the corner in the graph of $dt^*(\epsilon)$ at $\epsilon \approx .107764$. The top left figure presents a closer view of dt^* versus ϵ ; there is clearly a corner in the graph. The bottom left figure presents the magnitude of the imaginary part of the eigenvalue(s) that cross the unit circle. For ϵ close to, but smaller than, $\epsilon = .107764$, the instability arises when a single real-valued eigenvalue crosses the unit circle through the point -1 . For ϵ close to, but larger than, $\epsilon = .107764$, the instability arises when a complex conjugate pair of eigenvalues with nonzero imaginary part cross the unit circle. The plots to the right present the magnitudes of the eigenvalues as a function of dt for two values of ϵ close to $\epsilon = .107764$. The top plot is for an ϵ that is close to, but smaller than, $\epsilon = .107764$ and the bottom plot is for an ϵ value that is slightly larger than this critical value of ϵ . In both plots, there is a branch which denoted with a dot-dash line. This branch corresponds to a pair of complex conjugate eigenvalues; following this branch leftward and downward in the figure, one sees that it arose from the collision of two real-valued eigenvalues (there is a triple junction). In the top ($\epsilon = .107$) plot, the branch is to the right of the branch with one real eigenvalue: the complex pair of eigenvalues are not the cause of the stability restriction. In the bottom ($\epsilon = .109$) plot, the two branches have exchanged positions. If one views a sequence³ of such plots as ϵ increases from .107 to .109, one sees that both branches are moving rightward but that the branch that carries the single real eigenvalue is moving rightward at a slightly faster speed; as a result it overtakes the branch that carries the complex pair of eigenvalues. The difference in speeds is the cause of the corner in the graph of $dt^*(\epsilon)$.

Figure 6 is the analogue of Figure 5; it addresses the cause of the jump in the graph of $dt^*(\epsilon)$ at the critical value $\epsilon \approx 0.134504$. From the figure in the left, we see that there is a jump in the stability restriction dt^* and that the eigenvalues switch from a complex conjugate pair to a single real eigenvalue as ϵ increases through the critical value. The upper right plot presents the magnitude of the eigenvalues for a value of ϵ that is slightly smaller than the critical value and the bottom right plot presents them for a value that is slightly larger. In both

³The matlab source code is available at https://github.com/daveboat/vssimex_pnp. At that site, a curious reader can find a movie of plots like the left plot in Figure 4 as ϵ increases: `stability_roots.avi` and `stability_roots.mov`.

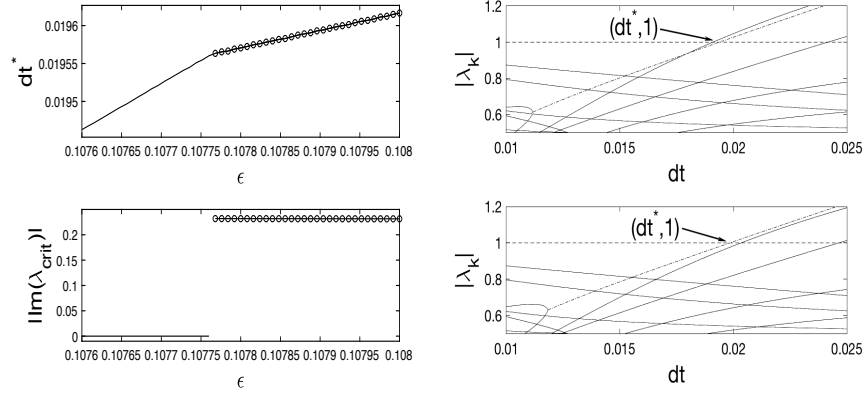


Figure 5: PNP-FBV system (1)–(8) with physical and numerical parameters identical to those used for Figure 1 except for ϵ , which varies. Left plot, top: dt^* versus ϵ where dt^* is found from the linear stability analysis. There is a corner in the graph at approximately $\epsilon = .107764$. Left plot, bottom: The magnitude of the imaginary part of the eigenvalue(s) on the unit circle. There is a jump at approximately $\epsilon = 0.107764$. Right plot, top: The magnitude of the eigenvalues of the linearized problem versus dt versus for $\epsilon = .107$. Right plot, bottom: The magnitude of the eigenvalues of the linearized problem versus dt versus for $\epsilon = .109$.

plots, we see that the triple point, where the branch carrying the complex pair of eigenvalues emerges from the intersection of two branches carrying single real eigenvalues, is close to the dashed line at height 1. In the upper plot, we see that the upper branch (before the triple point) is below the dashed line — the first eigenvalues to cross the unit circle are the complex pair, for a larger value of dt^* . However, as ϵ increases, this upper branch (before the triple point) moves upwards and it reaches the dashed line when $\epsilon \approx 0.134504$; at this value of ϵ , the stability restriction dt^* jumps downwards. After this critical value of ϵ , the stability restriction is due to a single real eigenvalue crossing the unit circle at -1 .

5.3. Dependence of stability domain on imposed voltage

We next study how the stability restriction, dt^* , depends on the imposed voltage. For this, we imposed constant voltages, with values ranging between 0 and 3.

The left plot of Figure 7 presents the stability domain, dt^* , versus ϵ for the four constant imposed voltages. We see that for smaller values of ϵ , dt^* does not appear to be affected as much by the imposed voltage compared to larger values of ϵ . The vertical dashed line in the upper left plot of Figure 7 indicates $\epsilon = .5$; it intersects the graphs of dt^* at the values 0.0250, 0.0223, 0.0191, and 0.0158. In the companion article [4], we presented the results of a simulation with a time-dependent imposed voltage; the imposed voltage was initially held constant at 0 and then transitioned quickly to the value 3 and held constant. As demonstrated in Figure 4 of the companion article [4], the VSSBDF2 adaptive time-stepper

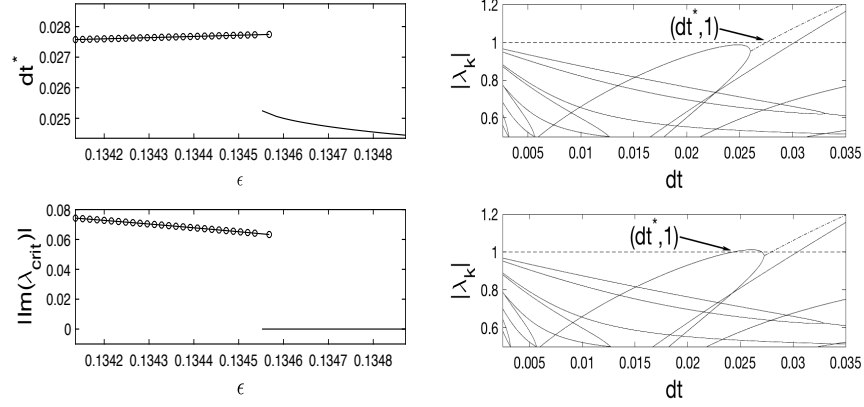


Figure 6: PNP-FBV system (1)–(8) with physical and numerical parameters identical to those used for Figure 1 except for ϵ , which varies. Left plot, top: dt^* versus ϵ where dt^* is found from the linear stability analysis. There is a jump at approximately $\epsilon \approx .134504$. Left plot, bottom: The magnitude of the imaginary part of the eigenvalue(s) on the unit circle. Right plot, top: The magnitude of the eigenvalues of the linearized problem versus dt versus for $\epsilon = .134$. Right plot, bottom: The magnitude of the eigenvalues of the linearized problem versus dt versus for $\epsilon = .135$.

had its time steps stabilize to $dt \approx 0.0250$ when the imposed voltage was 0 and then, after a transient, they stabilized to $dt \approx 0.0158$ after the imposed voltage was switched to 3.

The lower left plot of Figure 7 suggests that dt^* may be proportional to a power of ϵ for small values of ϵ . The right plot of Figure 7 presents $\ln(dt^*)$ versus $\ln(\epsilon)$. The four graphs appear to be roughly linear but do not appear to have the same slopes. All four plots correspond to dt^* decreasing to zero slightly faster than ϵ^2 , consistent with Table 2 in the companion article [4].

5.4. Dependence of stability domain on spatial discretization

We next consider the effect of the mesh on the stability restriction. The plot in the left of Figure 8 presents stability restrictions for four different meshes: one uniform mesh and three piecewise uniform meshes that have finer meshes near $x = 0, 1$. The stability restriction depends on the mesh in a mild manner. This is not surprising given that the critical eigenmodes of the linearized scheme presented in the bottom right plots of Figures 3 and 4 do not appear to have structures that need significant spatial resolution.

We find that the observed dependence is more like that of a reaction–diffusion equation than that of a diffusion equation. Consider a simple linear PDE: a diffusion equation with a sink $u_t = D u_{xx} - (\frac{1}{\epsilon^2}) u$ on $(0, 1)$ with Dirichlet boundary conditions $u(0, t) = u(1, t) = 0$. Choosing a simple spatial discretization, the resulting system of ODEs is easily diagonalized. Using the SBDF2 scheme with the diffusion term handled implicitly and the source term handled explicitly, one can find the stability restriction dt^* using the linear stability analysis in

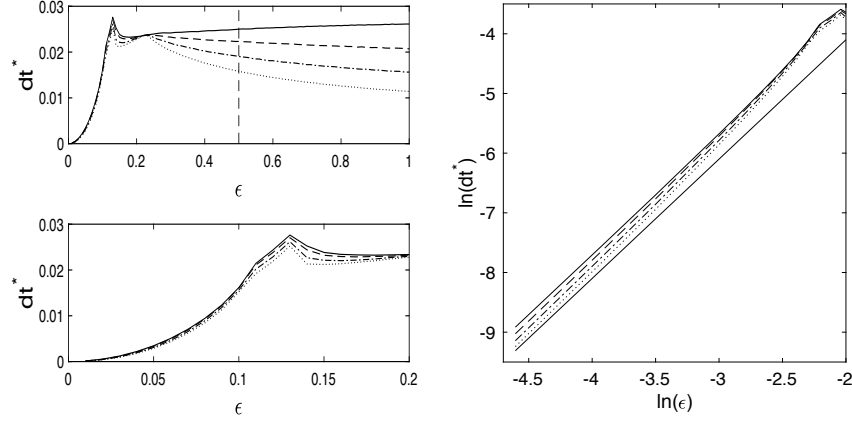


Figure 7: PNP-FBV system (1)–(8) with physical and numerical parameters identical to those used for Figure 1 except for ϵ , which varies, and the constant imposed voltage. Four values of (constant) imposed voltage are considered: $v(t) = 0, 1, 2$, and 3. Left plots: The stability restriction dt^* versus ϵ for $v(t) = 0$ (solid), $v(t) = 1$ (dashed), $v(t) = 2$ (dot-dashed), and $v(t) = 3$ (dotted). Right plot: Here, $\log(dt^*)$ is plotted versus $\log(\epsilon)$ for the same imposed voltage values and line notations. The decay is roughly like ϵ^2 ; fitting the data yields exponents 2.0677, 2.1145, 2.1540, and 2.1813 for constant imposed voltages $v(t) = 0, 1, 2$, and 3 respectively. A sight-line corresponding to $dt \propto \epsilon^2$ is provided (solid line).

Appendix A of [5]. One finds that that if $\epsilon^2 D |\lambda_1| < 3$ then the scheme is conditionally stable with $dt^* = 4/(D_1 \lambda_1 + 3/\epsilon^2)$. Otherwise the scheme is unstable. Here λ_1 is the first negative eigenvalue of the discretized Laplacian. For this example, we see that the stability restriction, dt^* , does depend on the mesh because λ_1 depends on the mesh. However, for a fixed ϵ , dt^* does not go to zero as the mesh is refined: dt^* converges to a positive number. If the time-step violates the stability restriction, the fastest growing mode is the eigenvector that approximates the low frequency eigenfunction $\sin(\pi x)$. We also note that $dt^* = 4/(D_1 \lambda_1 + 3/\epsilon^2) \sim \epsilon^2$ for $\epsilon \ll 1$.

5.5. Effect of Richardson Extrapolation

Richardson extrapolation is commonly used to increase the accuracy of time-stepping, however we have not found much discussion of its possible effect on numerical stability. Although we note that in [13], the authors present an analysis of a stabilized Euler time-stepping scheme for $u_t = -a u$ where $a > 0$. They demonstrate that their stabilization parameter b has a threshold value at which their scheme changes from conditionally stable to unconditionally stable. They also demonstrate how Richardson extrapolation affects that threshold value.

The adaptive time-stepper computes two approximations of the solution at time t^{n+1} . The solution at time t^{n+1} is then taken to equal the “coarse” approximation: \mathbf{u}_c^{n+1} ; see Section 3. The linear stability analysis is built upon

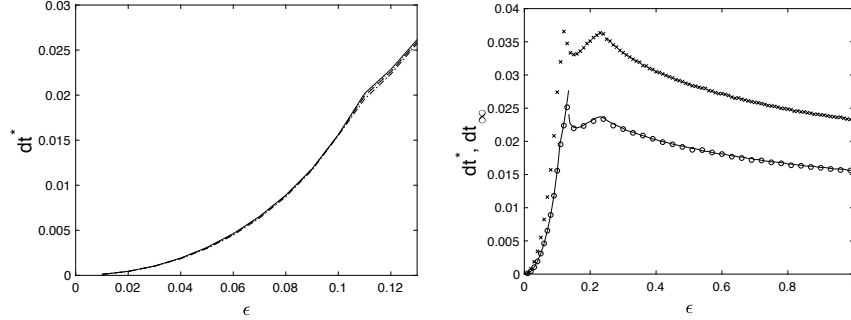


Figure 8: PNP-FBV system (1)–(8) with physical and numerical parameters identical to those used for Figure 1 except for ϵ , which varies. Left plot: For four different meshes, dt^* is computed and plotted against ϵ . Solid line: uniform mesh with $dx = 1/90$. Dot-dashed line: piecewise uniform mesh with $dx = 1/150$ in $[0, 1/10]$ and $[9/10, 1]$ and $dx = 4/75$ elsewhere. Dashed line: piecewise uniform mesh with $dx = 1/300$ in $[0, 1/10]$ and $[9/10, 1]$ and $dx = 2/75$ elsewhere. Dotted line: piecewise uniform mesh with $dx = 1/450$ in $[0, 1/10]$ and $[9/10, 1]$ and $dx = 4/225$ elsewhere. Right plot: The parameters are as in Figure 2. Solid line: dt^* versus ϵ where dt^* is found from the linear stability analysis. Open circles: dt_∞ as found by the time-step size stabilizing in the VSSBDF2 adaptive time-stepper with no Richardson extrapolation step. X-marks: dt_∞ as found by the VSSBDF2 adaptive time-stepper with a Richardson extrapolation step.

the solutions satisfying (13) and so its predictions only apply to the VSSBDF2 adaptive time-stepper when Richardson extrapolation is not used.

However, as described in [1, 4] and in Appendix A, one could use u_c^{n+1} and u_f^{n+1} to construct a more accurate approximation of $u(t^{n+1})$ via Richardson extrapolation. We find that when using the VSSBDF2 adaptive time-stepper with Richardson extrapolation on the PNP-FBV system, the observed behaviour is like that when Richardson extrapolation was not used: the time-steps stabilized at a value dt_∞ [5].

The plot in the right of Figure 8 presents dt^* and dt_∞ where dt_∞ is found using two different implementations of the VSSBDF2 adaptive time-stepper. The open circles denote dt_∞ as found by the VSSBDF2 adaptive time-stepper with no Richardson extrapolation. The crosses denote dt_∞ as found by the VSSBDF2 adaptive time-stepper with Richardson extrapolation. Because dt_∞ and dt^* agree closely when Richardson extrapolation is not used, we believe dt_∞ is a good proxy for the stability restriction dt^* when Richardson extrapolation is used. In the plot, the crosses are above the circles, sometimes markedly so, and for this reason the simulations finish more quickly when Richardson extrapolation is used. It is also interesting that the plot of dt_∞ versus ϵ when Richardson extrapolation is used (crosses) has a very similar shape to the plot of the data when it is not used (circles).

For the PNP-FBV system, we find that using Richardson extrapolation as part of the adaptive time-stepper leads to greater stability. However, this is problem dependent. For example, in [5], we find that if one repeats this exper-

iment for the diffusion equation $u_t = D_1 u_{xx} + D_2 u_{xx}$ then using Richardson extrapolation in the VSSBDF2 adaptive time-stepper can lead to *less* stability. For some choices of D_1 and D_2 , dt_∞ is smaller when Richardson extrapolation is used in the VSSBDF2 adaptive time-stepper. Also, there are choices of D_1 and D_2 for which the SBDF2 time-stepper is unconditionally stable (and so the VSSBDF2 adaptive time-stepper with no Richardson extrapolation has no stabilization to dt_∞) but if one uses Richardson extrapolation in the adaptive time-stepper then a limiting step size dt_∞ is observed. This suggests that, for such parameter choices, using Richardson extrapolation changes the underlying time-stepping scheme from unconditionally stable to conditionally stable.

6. Conclusions and Future Work

In this work, we considered the Poisson-Nernst-Planck equations with generalized Frumkin-Butler-Volmer reaction kinetics at the electrodes. When the VSSBDF2 adaptive time-stepper is being used to study scenarios in which the imposed voltage or the imposed current is (nearly) constant for long periods of time, the time-step sizes stabilize to a limiting value and the computed solutions “nearly” converge to a steady state. This behaviour is understood by linearizing the numerical scheme about the steady state. The linearized scheme is found to be conditionally stable, with a stability restriction that agrees with the time-step at which that the adaptive time-stepper stabilized. The stability domain’s dependence on the singular perturbation parameter ϵ is studied numerically and is found to have a corner and a jump discontinuity. The eigenfunctions corresponding to the critical eigenvalues are studied; the conditional stability is not related to a high-frequency instability. Using a Richardson extrapolation step in the adaptive time-stepper appears to stabilize the problem somewhat in that the limiting time-step is larger. However other systems are presented for which Richardson extrapolation can destabilize the scheme.

It would be interesting to see if one can modify, or remove, the conditional stability by using information about the structure of the steady state. For example, [7] created an unconditionally stable scheme for a nonlinear diffusion equation by using bounds on the solution, although the instability being controlled was due to high frequencies.

Our methods are not restricted to the PNP-FBV system or to the VSSBDF2 adaptive time-stepper. If one is using linear multi-step method to study a system that has asymptotically stable steady states, our approach is relevant. We expect that it would generalize in a natural manner to Runge-Kutta methods as well. A natural next step would be to study the stability properties of semi-implicit schemes beyond steady states by considering problems that have orbitally stable special solutions, such as travelling waves, or by considering problems that have asymptotically stable special solutions, such as self-similar solutions.

Appendix A. Overview of adaptive time-stepping scheme

Algorithm 1 shows our adaptive time-stepping scheme. This type of error control strategy is discussed in Chapter II.4 of Hairer, Norsett and Wanner [49].

Algorithm 1 Adaptive time-stepping scheme for a single time step

```

 $i \leftarrow 0$  ▷ Reset loop counter for this time step
 $dt_{\text{now}} \leftarrow dt_{\text{old}}$  ▷ Initial guess at  $dt$  for this time step
 $u_c^{n+1} \leftarrow \text{TimeStep}(dt_{\text{now}})$  ▷ Coarse step, TimeStep() using Eq. (11) or (A.2)
 $u_f^{n+1} \leftarrow \text{TimeStep}(dt_{\text{now}}/2)$  ▷ Fine step
 $\epsilon_c^i \leftarrow \text{Error}(dt_{\text{now}}, dt_{\text{old}}, u_c^{n+1}, u_f^{n+1})$  ▷ Error() from equation (12)
while  $\text{abs}(\epsilon_c^i - \text{tol}) > \text{range}$  do ▷ Loop until the error is acceptable
  if  $i \geq i_{\text{max}}$  then ▷ Enforce maximum iterations
     $u_c^{n+1} \leftarrow \text{TimeStep}(dt_{\text{min}})$ 
     $u_f^{n+1} \leftarrow \text{TimeStep}(dt_{\text{min}}/2)$ 
    break
  end if
   $dt_{\text{now}} \leftarrow \min \left( \max \left( \left( \frac{\text{tol}}{\epsilon_c^i} \right)^{1/p}, \eta_{\text{min}} \right), \eta_{\text{max}} \right) dt_{\text{now}}$  ▷ Update  $dt$ 
  if  $dt_{\text{now}} > dt_{\text{max}}$  then ▷ Enforce maximum time step
     $u_c^{n+1} \leftarrow \text{TimeStep}(dt_{\text{max}})$ 
     $u_f^{n+1} \leftarrow \text{TimeStep}(dt_{\text{max}}/2)$ 
    break
  end if
   $u_c^{n+1} \leftarrow \text{TimeStep}(dt_{\text{now}})$ 
   $u_f^{n+1} \leftarrow \text{TimeStep}(dt_{\text{now}}/2)$ 
   $\epsilon_c^{i+1} \leftarrow \text{Error}(dt_{\text{now}}, dt_{\text{old}}, u_c^{n+1}, u_f^{n+1})$  ▷ Update error estimate
   $i \leftarrow i + 1$ 
end while
if Richardson extrapolation is used then
   $u^{n+1} \leftarrow \alpha u_c^{n+1} + \beta u_f^{n+1}$  ▷  $\alpha$  and  $\beta$  are defined in equation (A.1)
else
   $u^{n+1} \leftarrow u_c^{n+1}$ 
end if

```

The p in the time-step update formula in the algorithm is the order of the local truncation error; $p = 3$ for VSSBDF2. Unless noted otherwise, the simulations in this article used $\text{tol} = 10^{-6}$, $\text{range} = \text{tol}/3$, $\eta_{\text{max}} = 1.1$, $\eta_{\text{min}} = .9$, $dt_{\text{max}} = 1$ and $dt_{\text{min}} = 10^{-8}$.

Richardson extrapolation uses a linear combination of u_f^{n+1} and u_c^{n+1} to construct an improved approximation u^{n+1} which has a smaller truncation error. Specifically, $u^{n+1} = \alpha u_c^{n+1} + \beta u_f^{n+1}$ with coefficients

$$\alpha = -\frac{dt_{\text{old}} + 3 dt_{\text{now}}}{7 dt_{\text{old}} + 5 dt_{\text{now}}} \quad \text{and} \quad \beta = 8 \frac{dt_{\text{old}} + dt_{\text{now}}}{7 dt_{\text{old}} + 5 dt_{\text{now}}}. \quad (\text{A.1})$$

The local truncation error for u^{n+1} is one order higher than the local truncation errors for u_c^{n+1} and u_f^{n+1} [1, 4]. Note that if $dt_{\text{now}} = dt_{\text{old}}$, then (A.1) reduces to the standard Richardson extrapolation formula for second-order schemes.

Since we are using a two-step time-stepping scheme, for the first time-step, we use a one-step semi-implicit scheme

$$\frac{1}{dt} (u^1 - u^0) = f(u^0) + g(u^1), \quad (\text{A.2})$$

along with the error estimate $\epsilon_c^1 = (4/3)(u_c^1 - u_f^1)$, the time-step update formula with $p = 2$, and the extrapolation formula $u^1 = 2u_f^1 - u_c^1$.

Appendix B. Acknowledgements

Research supported in part by NSERC grant OGP06617.

We thank Greg Lewis, Keith Promislow, Steve Ruuth, Adam Stinchcombe, and Brian Wetton for helpful conversations and encouragement. We thank the reviewers of an earlier version of this article for their careful, thorough comments and suggestions.

References

- [1] David Yan. Macroscopic Modeling of a One-Dimensional Electrochemical Cell Using the Poisson-Nernst-Planck Equations. PhD thesis, University of Toronto, 2017.
- [2] David Yan, Martin Z. Bazant, P.M. Biesheuvel, Mary C. Pugh, and Francis P. Dawson. Theory of linear sweep voltammetry with diffuse charge: Unsupported electrolytes, thin films, and leaky membranes. Phys. Rev. E, 95:033303, Mar 2017.
- [3] D. Wang and S.J. Ruuth. Variable step-size implicit-explicit linear multi-step methods for time-dependent partial differential equations. J. Comput. Math., 26(6):838–855, 2008.
- [4] David Yan, Mary C. Pugh, and Francis P. Dawson. Adaptive time-stepping schemes for the solution of the Poisson-Nernst-Planck equations. arXiv:1703.10297, 2019.
- [5] Mary C. Pugh, David Yan, and Francis P. Dawson. A study of the numerical stability of an imex scheme with application to the Poisson-Nernst-Planck equations. arXiv:1905.01368 [v1], 2019.
- [6] Rodolfo R. Rosales, Benjamin Seibold, David Shirokoff, and Dong Zhou. Unconditional Stability for Multistep ImEx Schemes: Theory. SIAM J. Numer. Anal., 55(5):2336–2360, 2017.

- [7] Benjamin Seibold, David Shirokoff, and Dong Zhou. Unconditional stability for multistep ImEx schemes: Practice. J. Comput. Phys., 376:295–321, JAN 1 2019.
- [8] Georgios Akrivis and Fotini Karakatsani. Modified implicit-explicit BDF methods for nonlinear parabolic equations. BIT, 43(3):467–483, 2003.
- [9] Georgios Akrivis, Ohannes Karakashian, and Fotini Karakatsani. Linearly implicit methods for nonlinear evolution equations. Numer. Math., 94(3):403–418, 2003.
- [10] J Frank, W Hundsdorfer, and JG Verwer. On the stability of implicit-explicit linear multistep methods. Appl. Numer. Math., 25(2-3):193–205, NOV 1997. Workshop on Innovative Time Integrators, CTR MATH & COMP SCI, AMSTERDAM, NETHERLANDS, OCT 30-NOV 01, 1996.
- [11] Jim Douglas, Jr. and Todd Dupont. Alternating-direction Galerkin methods on rectangles. In Numerical Solution of Partial Differential Equations, II (SYNSPADE 1970) (Proc. Sympos., Univ. of Maryland, College Park, Md., 1970), pages 133–214. Academic Press, New York, 1971.
- [12] Thomas Y. Hou, John S. Lowengrub, and Michael J. Shelley. Removing the stiffness from interfacial flows with surface tension. J. Comput. Phys., 114(2):312–338, 1994.
- [13] Laurent Duchemin and Jens Eggers. The Explicit-Implicit-Null method: Removing the numerical instability of PDEs. J. Comput. Phys., 263:37–52, APR 15 2014.
- [14] Assyr Abdulle and Alexei A. Medovikov. Second order Chebyshev methods based on orthogonal polynomials. Numer. Math., 90(1):1–18, 2001.
- [15] Jaemin Shin, Hyun Geun Lee, and June-Yub Lee. Unconditionally stable methods for gradient flow using convex splitting Runge-Kutta scheme. J. Comput. Phys., 347:367–381, 2017.
- [16] G. Izzo and Z. Jackiewicz. Highly stable implicit-explicit runge-kutta methods. Appl. Numer. Math., 113:71–92, 2017.
- [17] Aly-Khan Kassam and Lloyd N. Trefethen. Fourth-order time-stepping for stiff PDEs. SIAM J. Sci. Comput., 26(4):1214–1233, 2005.
- [18] Lili Ju, Jian Zhang, Liyong Zhu, and Qiang Du. Fast explicit integration factor methods for semilinear parabolic equations. J. Sci. Comput., 62(2):431–455, 2015.
- [19] Paul A. Milewski and Esteban G. Tabak. A pseudospectral procedure for the solution of nonlinear wave equations with examples from free-surface flows. SIAM J. Sci. Comput., 21(3):1102–1114, 1999.

- [20] Michael L. Minion. Semi-implicit spectral deferred correction methods for ordinary differential equations. Commun. Math. Sci., 1(3):471–500, 2003.
- [21] Oscar P. Bruno and Edwin Jimenez. Higher-Order Linear-Time Unconditionally Stable Alternating Direction Implicit Methods for Nonlinear Convection-Diffusion Partial Differential Equation Systems. J. Fluids Eng.-Trans. ASME, 136(6), JUN 2014.
- [22] Oscar P. Bruno and Mark Lyon. High-order unconditionally stable FC-AD solvers for general smooth domains. I. Basic elements. J. Comput. Phys., 229(6):2009–2033, 2010.
- [23] Mark Lyon and Oscar P. Bruno. High-order unconditionally stable FC-AD solvers for general smooth domains. II. Elliptic, parabolic and hyperbolic PDEs; theoretical considerations. J. Comput. Phys., 229(9):3358–3381, 2010.
- [24] P.M. Biesheuvel and M.Z. Bazant. Nonlinear dynamics of capacitive charging and desalination by porous electrodes. Phys. Rev. E, 81(3):031502, 2010.
- [25] P.M. Biesheuvel, Yeqing Fu, and M.Z. Bazant. Diffuse charge and Faradaic reactions in porous electrodes. Phys. Rev. E, 83(6):061507, 2011.
- [26] P.M. Biesheuvel, Yeqing Fu, and M.Z. Bazant. Electrochemistry and capacitive charging of porous electrodes in asymmetric multicomponent electrolytes. Russ. J. Electrochem., 48(6):580–591, 2012.
- [27] P.B. Peters, R. van Roij, Martin Z. Bazant, and P.M. Biesheuvel. Analysis of electrolyte transport through charged nanopores. Phys. Rev. E, 93:053108, 2016.
- [28] Ian Streeter and Richard G. Compton. Numerical simulation of potential step chronoamperometry at low concentrations of supporting electrolyte. J. Phys. Chem. C, 112(35):13716–13728, 2008.
- [29] Richard G. Compton and Craig E. Banks. Understanding Voltammetry. Imperial College Press, London, 2011.
- [30] E. Victoria Dydek and Martin Z. Bazant. Nonlinear dynamics of ion concentration polarization in porous media: The leaky membrane model. AIChE Journal, 59(9):3539–3555, 2013.
- [31] Victor V. Nikonenko, Natalia D. Pismenskaya, Elena I. Belova, Philippe Sistat, Patrice Huguët, Gérald Pourcelly, and Christian Larchet. Intensive current transfer in membrane systems: Modelling, mechanisms and application in electrodialysis. Adv. Colloid Interface Sci., 160(1):101–123, 2010.

- [32] A. Yaroshchuk. Over-limiting currents and deionization shocks in current-induced polarization: local equilibrium analysis. Adv. Colloid Interface Sci., 183:68–81, 2012.
- [33] Martin Z. Bazant and Todd M. Squires. Induced-charge electrokinetic phenomena. Curr. Opin. Colloid Interface Sci., 15(3):203–213, 2010.
- [34] Martin Z. Bazant, Mustafa Sabri Kilic, Brian D. Storey, and Armand Ajdari. Towards an understanding of induced-charge electrokinetics at large applied voltages in concentrated solutions. Adv. Colloid Interface Sci., 152(1):48–88, 2009.
- [35] Martin Z. Bazant, Brian D. Storey, and Alexei A. Kornyshev. Double layer in ionic liquids: Overscreening versus crowding. Phys. Rev. Lett., 106(4):046102, 2011.
- [36] Alexei A. Kornyshev. Double-layer in ionic liquids: Paradigm change? J. Phys. Chem. B, 111:5545–5557, 2007.
- [37] Martin Z. Bazant, Kevin T. Chu, and B.J. Bayly. Current-voltage relations for electrochemical thin films. SIAM J. Appl. Math., 65(5):1463–1484, 2005.
- [38] Kevin T. Chu and Martin Z. Bazant. Electrochemical thin films at and above the classical limiting current. SIAM J. Appl. Math., 65(5):1485–1505, 2005.
- [39] P.M. Biesheuvel, M. van Soestbergen, and M.Z. Bazant. Imposed currents in galvanic cells. Electrochim. Acta, 54:4857–4871, 2009.
- [40] P. Maarten Biesheuvel, Alejandro A. Franco, and Martin Z. Bazant. Diffuse charge effects in fuel cell membranes. J. Electrochem. Soc., 156(2):B225–B233, 2009.
- [41] Alpha A Lee, Svyatoslav Kondrat, Gleb Oshanin, and Alexei A Kornyshev. Charging dynamics of supercapacitors with narrow cylindrical nanopores. Nanotechnology, 25(31):315401, 2014.
- [42] Martin Z. Bazant. Theory of chemical kinetics and charge transfer based on nonequilibrium thermodynamics. Accounts Chem. Res., 46(5):1144–1160, 2013.
- [43] M. van Soestbergen. Frumkin-Butler-Volmer theory and mass transfer in electrochemical cells. Russ. J. Electrochem., 48(6):570–579, 2012.
- [44] A.A. Moya, J. Castilla, and J. Horno. Ionic transport in electrochemical cells including electrical double-layer effects. A network thermodynamics approach. J. Phys. Chem., 99:1292–1298, 1995.
- [45] M. van Soestbergen, P.M. Biesheuvel, and M.Z. Bazant. Diffuse-charge effects on the transient response of electrochemical cells. Phys. Rev. E, 81(2):1–13, 2010.

- [46] U.M. Ascher, S.J. Ruuth, and B.T.R. Wetton. Implicit-explicit methods for time-dependent partial differential equations. SIAM J. Numer. Anal., 32(3):797–823, 1995.
- [47] J. Rosam, P.K. Jimack, and A. Mullis. A fully implicit, fully adaptive time and space discretisation method for phase-field simulation of binary alloy solidification. J. Comput. Phys., 225(2):1271–1287, 2007.
- [48] R.J. LeVeque. Finite Difference Methods for Ordinary and Partial Differential Equations: Steady-State and Time-Dependent Problems. SIAM, Philadelphia, 2007.
- [49] Ernst Hairer, Syvert P. Nørsett, and Gerhard Wanner. Solving Ordinary Differential Equations I: Nonstiff Problems (Springer Series In Computational Mathematics). Springer Berlin, Heidelberg, 2009.